proceedings

MDPI

Proceedings

Attainment of Pentagonal-Bipyramidal Ln^{III} Complexes from a Planar Pentadentate Ligand †

Julio Corredoira-Vázquez, Matilde Fondo, Jesús Sanmartín-Matalobos and Ana M. García-Deibe *

Departamento de Química Inorgánica, Facultade de Química. Campus Vida. Universidade de Santiago de Compostela, 15782 Santiago de Compostela, Spain; julio_corredoira@hotmail.com (J.C.-V.); matilde.fondo@usc.es (M.F.); jesus.sanmartin@usc.es (J.S.-M.)

* Correspondence: ana.garcia.deibe@usc.es; Tel.: +34-981-814-237

† Presented at the 2nd International Electronic Conference on Crystals, 10–20 November 2020; Available online: https://iocc_2020.sciforum.net/.

Published: 30 December 2020

Abstract: The search for mononuclear lanthanoid-based single-ion magnets (SIMs) has increased the interest in some coordination environments with low coordination numbers, in combination with an axial symmetry, as they could maximize the anisotropy of complexes of oblate lanthanoid ions, such as dysprosium(III). In this sense, the pentagonal–bipyramid geometry can have ground-state doublets with perfect axiality, and therefore such complexes can be good candidates for SIMs. In our particular case, we have used a well-known open planar pentadentate chelating Schiff base ligand as 2,6-bis(1-salicyloylhydrazonoethyl)pyridine) (H_4daps) for the synthesis of air-stable pentagonal–bipyramidal Ln^{III} complexes (these being Ln: Dy and Er, oblate and prolate, respectively), in order to compare their structures. Thus, the reaction of H_4daps with $(CH_3)_4NOH{\cdot}5H_2O$ and the corresponding $LnCl_3$·hexahydrate has yielded heptacoordinate $[(CH_3)_4N][Ln^{III}(H_2daps)Cl_2]$ complexes, where the tetramethylammonium cation is acting as the counterion of pentagonal–bipyramidal Ln^{III} complexes, which are bearing two chloride atoms in apical positions. As both complexes could be crystallized as single crystals, we can compare their crystal structures, as well as with some other related complexes in the literature, which contain different counterions, trying to see their influence on other properties of the compounds, such as their magnetic behavior.

Keywords: lanthanoid; dysprosium(III); erbium(III); pentagonal–bipyramidal coordination environment; pentadentate ligand; hydrazone; Schiff base

1. Introduction

Since the discovery of the first single-ion magnet (SIM) in 2003 [1], and the realization that the control of anisotropy is the key factor for the isolation of single molecule magnets (SMMs), the field of molecular magnetism has begun to focus on the lanthanoid elements, since they present intrinsic anisotropy. However, the anisotropy of the whole molecule is modulated by the interaction between the single-ion electron density and the crystal field environment in which it is placed, as Reinhart and Long have predicted [2]. In this sense, for oblate ions, a strong axial crystal field should maximize the uniaxial anisotropy, while for prolate ions, a strong crystal field in the equatorial plane is preferable. Accordingly, dysprosium should maximize its anisotropy in a lineal environment [3]. However, lanthanoids hardly stabilize the coordination number 2, unless with very bulky ligands, as occurs in metallocenes, which hold the record of blocking temperature (80 K) [3], although they are not air-stable.

In the absence of air-stable complexes with coordination number 2, the coordination number 7, with pentagonal–bipyramidal (pbp) geometry, was the most explored one, leading to the blocking temperature record for an air-stable complex of 20 K [4]. Therefore, in order to improve the magnetic behavior of this kind of complex, more research is still needed in this area. With these considerations in mind, in this study we will describe the synthesis and magnetic characterization of a dysprosium and an erbium complex with pbp geometry, derived from a well-known planar pentadentate donor.

2. Materials and Methods

All chemical reagents were purchased from commercial sources and used as received without further purification. Elemental analyses of C, H and N were performed on a Carlo Erba EA 1108 analyzer. Infrared spectra were recorded in the ATR mode on a Varian 670 FT/IR spectrophotometer in the range of 4000–500 cm^{-1}. ^1H NMR spectra of 2,6-bis(1-salicyloylhydrazonoethyl)pyridine) (H_4daps) were recorded on a Bruker DPX-250 spectrometer**.**

H_4daps was obtained via a variation of a previously described method [5], using methanol as the solvent instead of benzene, and it was satisfactorily characterized by ^1H NMR spectroscopy.

2.1. Syntheses of the Complexes

Both $(CH_3)_4N[Ln(H_2daps)Cl_2]$ (Ln = Dy, Er) complexes were obtained in the same way, which is exemplified by the isolation of $(CH_3)_4N[Dy(H_2daps)Cl_2]$ (**DyH_2daps**). To a suspension of H_4daps (0.100 g, 0.232 mmol) in THF (25 mL), $(CH_3)_4NOH{\cdot}5H_2O$ (0.087 g, 0.463 mmol) and 27 mL of CH_3CN were added. The mixture was stirred for 30 min at 35 °C, and a yellow solution was obtained. $DyCl_3{\cdot}6H_2O$ (0.087 g, 0.232 mmol) was added to the solution, and the new mixture was stirred for 4 h at room temperature. The resulting solution was concentrated up to half of its volume, and the evaporation of this concentrated solution yielded single crystals of $(CH_3)_4N[Dy(H_2daps)Cl_2]$ after 24 h. The crystals were filtered and dried in air. Yield: 0.125 g (73%). Elemental analysis calcd. for $C_{27}H_{31}Cl_2DyN_6O_4$ (736.98): C, 43.96; N 11.40; H 4.21%. Found: C, 43.25; N, 11.39; H, 4.85%. IR (ATR, $\tilde{\nu}/cm^{-1}$): 1594 (amide I), 1523 (amide II), 3363 (OH). Crystal data deposited as CCDC 1841520.

$(CH_3)_4N[Er(H_2daps)Cl_2]$ (**ErH_2daps**): quantity of $ErCl_3{\cdot}6H_2O$ (0.088 g, 0.232 mmol). Single crystals of $(CH_3)_4N[Er(H_2daps)Cl_2]$ were obtained in the same way as those of **DyH_2daps**. Yield: 0.036 g (21%). Elemental analyses calcd. for $C_{27}H_{31}Cl_2ErN_6O_4$ (741.74): C, 43.68; N 11.32; H 4.18%. Found: C, 43.36; N, 11.36; H, 4.75%. IR (ATR, $\tilde{\nu}/cm^{-1}$): 1586 (amide I), 1521 (amide II), 3367 (OH). Crystal data deposited as CCDC 1841522.

2.2. X-ray Studies

Single crystals of $(CH_3)_4N[Dy(H_2daps)Cl_2]$ and $(CH_3)_4N[Er(H_2daps)Cl_2]$ were obtained as detailed above. Data were collected at 225 K on a Bruker Kappa APEXII CCD diffractometer, employing graphite monochromatized Mo-K_a (l = 0.71073 Å) radiation. Multi-scan absorption corrections were applied using SADABS [6]. These structures were solved by standard direct methods, employing SHELXT [7], and then were refined by full-matrix least-squares techniques on F^2, using SHELXL [8] from the program package SHELX-2014 [9]. The main crystal data are presented in Table 1.

All non-hydrogen atoms corresponding to the cationic complexes were anisotropically refined. Hydrogen atoms were typically included in the structure factor calculations in geometrically idealized positions. In contrast, those hydrogen atoms attached to the oxygen and/or nitrogen atoms of the ligands were found in the corresponding Fourier maps, and then either they were freely refined, or with thermal parameters derived from the parent atoms.

Powder diffractograms of **DyH_2daps** and **ErH_2daps** were recorded in a Philips diffractometer with a PW1710 control unit, a vertical PW1820/00 goniometer and an Enraf Nonius FR590 generator, operating at 40 kV and 30 mA, using monochromatized Cu-Kα (λ = 1.5418 Å) radiation. A scan was performed in the range $5 < 2\theta < 28.5°$ with t = 10 s and $\Delta 2\theta = 0.02°$. LeBail refinement was obtained with the aid of HighScore Plus Version 3.0d.

Table 1. Crystal data and structure refinement for **DyH$_2$daps** and **ErH$_2$daps**.

	$(CH_3)_4N[Dy(H_2daps)Cl_2]$	**$(CH_3)_4N[Er(H_2daps)Cl_2]$**
Formula	$C_{27}H_{31}Cl_2DyN_6O_4$	$C_{27}H_{31}Cl_2ErN_6O_4$
Molecular Weight	736.98	741.74
Temperature (K)	225(2)	250(2)
Crystal system	Orthorhombic	Orthorhombic
Space group	*C m c* 2$_1$	*C m c* 2$_1$
a (Å)	17.8879(9)	17.8142(18)
b (Å)	14.3964(7)	14.5177(14)
c (Å)	12.2189(6)	12.1790(14)
Volume (Å^3)	3146.6(3)	3149.7(6)
Z	4	4
Absorp. Coef. (mm^{-1})	2.585	2.874
Reflections collected	28,494	17,722
Independent reflections	3529 (R_{int} = 0.0353)	4710 (R_{int} = 0.0391)
Data/restraints/param.	3529/1/200	4710/1/201
Final *R* indices [$I > 2\sigma(I)$]	R_1 = 0.0268, wR_2 = 0.0534	R_1 = 0.0327, wR_2 = 0.0654
R indices (all data)	R_1 = 0.0328, wR_2 = 0.0560	R_1 = 0.0420, wR_2 = 0.0691

2.3. Magnetic Measurements

Magnetic susceptibility dc and ac measurements for powder crystalline samples of **DyH$_2$daps** and **ErH$_2$daps** were carried out with a Quantum Design SQUID MPMS-XL susceptometer. The magnetic susceptibility data were recorded under magnetic fields of 1000 Oe in the range 2–300 K. Magnetization measurements at 2.0 K were recorded under magnetic fields ranging from 0 to 50,000 Oe. Diamagnetic corrections were estimated from Pascal's Tables. Alternating current (ac) susceptibility measurements in different applied static fields (H_{dc} = 0 or 1000) were performed with an oscillating ac field of 4 Oe and an ac frequency of 1400 Hz for both complexes. In the case of **DyH$_2$daps**, the ac susceptibility measurements were additionally recorded under a dc field of 1000 Oe at ac frequencies ranging from 10 to 1488 Hz.

3. Results and Discussion

The complexes $(CH_3)_4N[Ln(H_2daps)Cl_2]$ (Ln = Dy, Er) were obtained as summarized in Scheme 1. Thus, the reaction of a suspension of H_4daps in THF with tetramethylamonium hydroxide, followed by the addition of $LnCl_3{\cdot}6H_2O$ at room temperature, gave rise to a yellow solution that, after concentration and slow evaporation, yielded single crystals of the **LnH$_2$daps**, which proved to be suitable for X-ray diffraction studies. This method of isolation of the complexes differs from that previously reported for $(CH_3CH_2)_3NH[Ln(H_2daps)Cl_2]$ (Ln = Tb, Dy) [10], since in our case the syntheses were carried out using less solvent at room temperature instead of reflux, but with an improved yield (73% compared to 64% for related $(CH_3CH_2)_3NH[Dy(H_2daps)Cl_2]$).

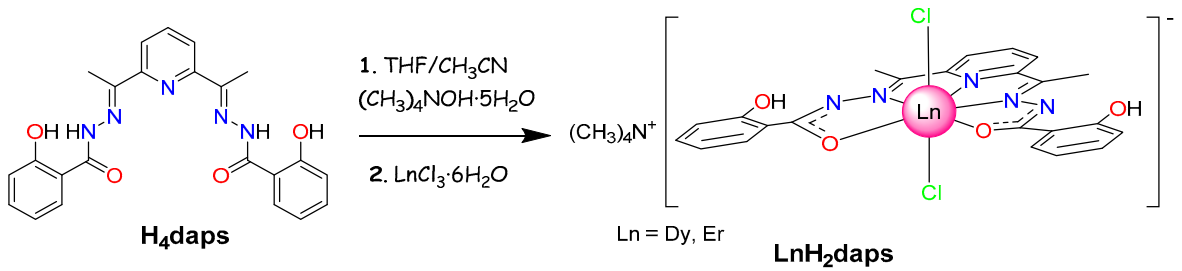

Scheme 1. Reaction scheme for the isolation of complexes **LnH$_2$daps.**

The complexes could be unequivocally characterized by elemental analysis, IR spectroscopy, and by X-ray diffraction techniques, and their magnetic behavior was also analyzed.

The infrared spectra of the compounds show two intense bands at ca. 1590 and 1520 cm^{-1}, which can be assigned to the amide I [ν(C=O)] and the amide II [δ(NH) + ν(C=N)] vibrations, respectively [5,11–13]. These bands experience significant negative shifts ranging from 30 to 65 cm^{-1} with respect to free H_4daps, which is consistent with the coordination of both carbonyl and both imine groups to the metal centers [5,10–13]. The spectra also show the presence of a fairly broad band centered at about 3360 cm^{-1}, which can be assigned to OH vibrations, in agreement with the non-deprotonation of the phenolic groups.

3.1. Crystal Structures

Despite multiple attempts to record the data and solve the structures of both complexes at a lower temperature of 100 K, these processes proved to be unsuccessful, so they were finally recorded at 225 and 250 K. The reason for this problem appears to be related to the modulated crystal structures [14], which avoid a satisfactory solution at low temperature, even using disorder models which mostly affect the $(CH_3)_4N^+$ counterion.

The structures of both compounds at 225 and 250 K are highly similar, as the ellipsoid diagrams shown in Figure 1 demonstrate. The main bond distances and angles are summarized in Table 2. Their crystal structures are also very similar to those described for the $Et_3NH[M(H_2daps)Cl_2]$ (M = Tb, Dy and Y) complexes [10].

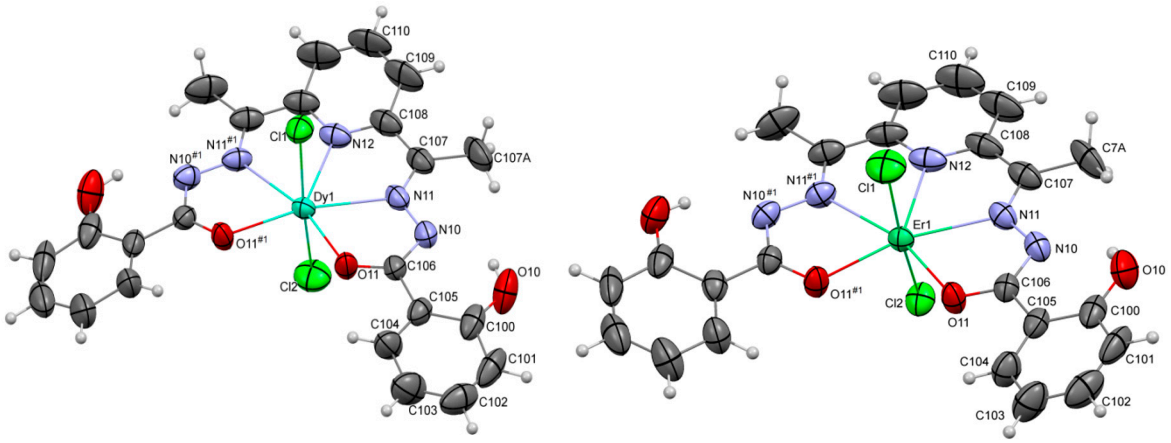

Figure 1. Ellipsoids diagram (50% probability) for $[Dy(H_2daps)Cl_2]^-$ and $[Er(H_2daps)Cl_2]^-$ anions in **DyH$_2$daps** and **ErH$_2$daps**. The $(CH_3)_4N^+$ counterions have been omitted for clarity.

Table 2. Main bond distances (Å) and angles (º) for **DyH$_2$daps** and **ErH$_2$daps.**

Dy1-O11	**2.253(4)**	**Er1-O11**	**2.238(4)**
Dy1-N12	2.426(8)	Er1-N12	2.418(8)
Dy1-N11	2.449(5)	Er1-N13	2.426(5)
Dy1-Cl2	2.613(2)	Er1-Cl1	2.585(3)
Dy1-Cl1	2.623(2)	Er1-Cl2	2.604(3)
Cl2-Dy1-Cl1	171.44(9)	Cl2-Er1-Cl1	171.73(10)
$O11^{\#1}$-Dy1-O11	98.94(18)	$O11^{\#1}$-Er1-O11	96.36(19)
O11-Dy1-N11	65.38(15)	O11-Er1-N11	66.00(15)
N12-Dy1-N11	65.17(11)	N11-Er1-N12	65.85(12)

Thus, the unit cells of both the complexes contain $[Ln(H_2daps)Cl_2]^-$ (Ln = Dy or Er) anions and $(CH_3)_4N^+$ cations, where two of the CH_3 groups are disordered over two sites. The $[Ln(H_2daps)Cl_2]^-$ anion is bisected by a crystallographic plane that contains the lanthanoid atom, the chloride ligands and the pyridine nitrogen atom, thus making both halves of the bisdeprotonated H_2daps^{2-} ligand equivalent. This donor acts as pentadentate, using the $N_{pyridine}$, N_{imine} and $O_{carbonyl}$ atoms to bind the Ln^{III} ion. Accordingly, H_2daps^{2-} provides an N_3O_2 environment to the metal center. The coordination

sphere of the lanthanoid atom is completed by two chloride anions. Therefore, the coordination number for the metal ion is 7, with slightly distorted pentagonal–bipyramidal geometry. The N_3O_2 core is nearly in a perfect plane, the main deviation of any atom from the calculated equatorial plane being of ca. 0.035 Å for **DyH$_2$daps** and 0.044 Å for **ErH$_2$daps**, and the metal center lying 0.003 (Dy) or 0.01 Å (Er) above the plane. The arrangement of the pentadentate ligand around the metal center is reinforced by typical intramolecular H bonds between the phenol moiety and the amine nitrogen atom N10.

In the pseudo pentagonal–bipyramid, the angles around the metal ion differ from the ideal values of 180 and 72°, the main distortion arising from the O–Dy–O angle of the equatorial plane (98.94(18)° for **DyH$_2$daps** and 93.36(19)° for **ErH$_2$daps**). In spite of this, all the distances and angles are within their normal range [10,13,15], but it should be noted that the Dy–$N_{pyridine}$ distance is a bit shorter than in the related $Et_3NH[Dy(H_2daps)Cl_2]$ [10], and that the Cl–Dy–Cl angle is notably less deviated from 180 in **DyH$_2$daps** (171.44(9)°) than in $Et_3NH[Dy(H_2daps)Cl_2]$ (166.32(6)°), showing that the cationic counterion could have an important influence on the structural parameters of the anionic complex. This may be related with the N-H···Cl interaction between the Et_3NH^+ cation and one of the chloride ligands.

Finally, the comparison of the experimental powder X-ray diffractogram of the crystalline products at room temperature with the calculated ones from the single X-ray diffraction data (Figure 2) at 298 K demonstrates that both products have been obtained with high purity, and that the collected samples and the solved single crystals are the same compounds, with the same structure.

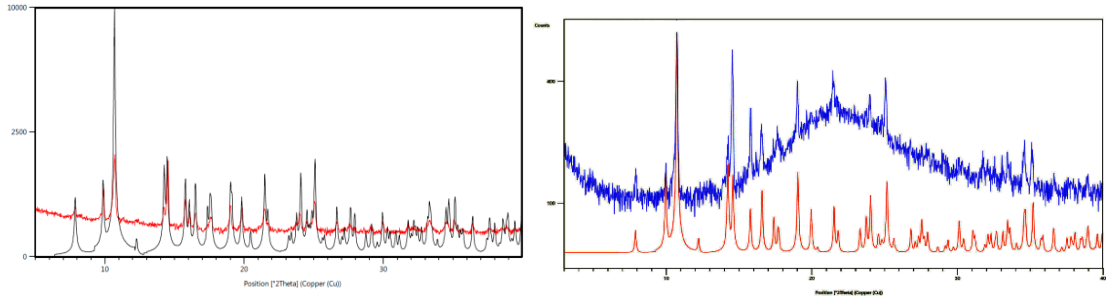

Figure 2. X-ray powder diffraction for: (**left**) **DyH$_2$daps** (red) and simulation from single X-ray data at 225 K (black); (**right**) **ErH$_2$daps** (blue) and simulation from single X-ray data at 250 K (red).

3.2. Magnetic Properties

Direct current (dc) magnetic susceptibility measurements were recorded for **DyH$_2$daps** and **ErH$_2$daps.** The plot for $\chi_M T$ vs. T for **DyH$_2$daps** is shown in Figure 3, as an example. At 300 K, the $\chi_M T$ vs. T is 13.1 $cm^3 Kmol^{-1}$, a value similar to but a bit lower than that expected for one isolated Dy^{3+} ion. This led to attempts to record the magnetic data newly, which allowed for discovering that the magnetic data were not reproducible, in spite of the high purity of the sample. This seems to be related with the changes in the crystal structure below 225 K. Thus, the fresh sample, if it is measured from 300 to 2 K, gives a $\chi_M T$ vs. T curve that differs from that recorded from 2 to 300 K, or from the one recorded from 300 to 2 K once the sample was previously cooled to 2 K, and the same phenomenon was also observed for **ErH$_2$daps**.

Despite this disadvantage that does not allow an accurate interpretation of the magnetic results, ac magnetic measurements were recorded in order to know the potentiality of these complexes as molecular magnets. Thus, alternating current (ac) magnetic susceptibility measurements were initially recorded under a zero external field at a frequency of 1400 Hz. In this case, none of the compounds show out-of-phase ac susceptibility (χ''_M) peaks. However, in the presence of an applied field of 1000 Oe, **ErH$_2$daps** still lacks χ''_M peaks, while **DyH$_2$daps** shows an ac susceptibility frequency and field dependence below 12 K (Figure 4). Thus, these data reveal that **DyH$_2$daps** is a field-induced SIM, while **ErH$_2$daps** is not.

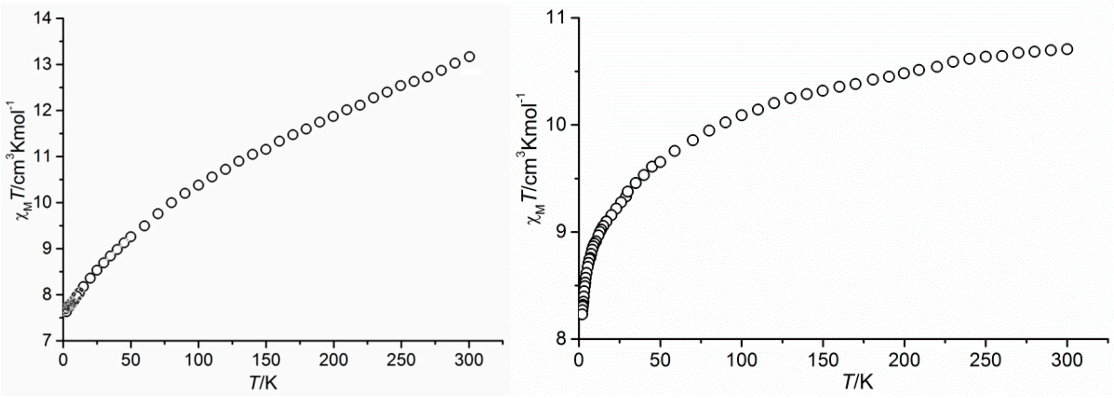

Figure 3. $\chi_M T$ vs. T for **DyH$_2$daps**: (**left**) a fresh sample, recorded from 300 to 2 K; (**right**) a fresh sample, recorded from 2 to 300 K.

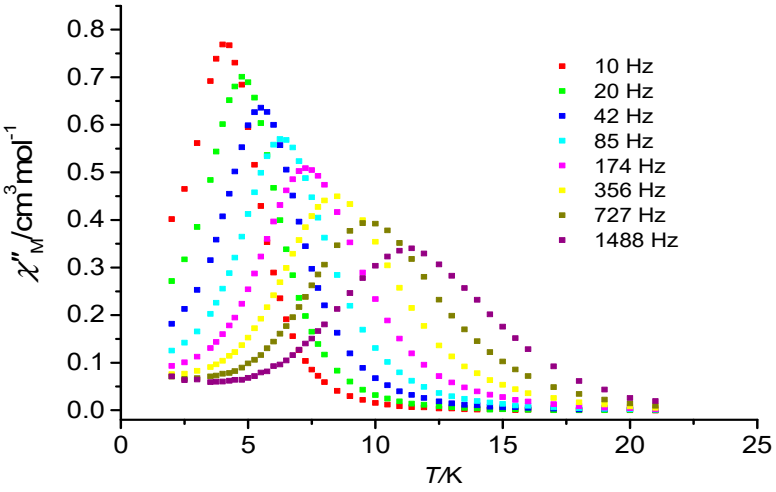

Figure 4. Temperature dependence of χ''_M for **DyH$_2$daps** in H_{dc} = 1000 Oe at different frequencies.

Despite the ac results for **DyH$_2$daps**, the data could not be properly analyzed, because, as previously discussed, these data are not completely reproducible, and no more ac parameters could be calculated.

4. Conclusions

Two pentagonal–bipyramidal Dy and Er complexes were obtained with high purity and fully characterized. The complexes undergo changes in their structures below 225 K, which seem related to the tetramethylammonium counterion, since such changes had not been described for similar complexes with triethylammonium counterions. Accordingly, this work demonstrates that it is easy to obtain pentagonal–bipyramidal complexes using H$_4$daps as a ligand, but that the stability of the formed anionic complexes seems to depend on the counterion. A rigorous magnetic analysis of the complexes is hampered by these changes in the structure at low temperatures, but, in spite of this, the ac measurements clearly show that the **DyH$_2$daps** is a field-induced SIM, while **ErH$_2$daps** lacks SIM behavior even in the presence of an external dc field of 1000 Oe.

Funding: This research was funded by Spanish Ministerio de Innovación, Ciencia y Universidades grant number [PGC2018 102052-B-C21].

Acknowledgments: Authors thank the Ministerio de Innovación, Ciencia y Universidades for financial support. J.C.-V thanks Xunta de Galicia for his Ph.D. fellowship.

Conflicts of Interest: The authors declare no conflict of interest.

References

1. Ishikawa, N.; Sugita, M.; Ishikawa, T.; Koshihara, S.; Kaizu, Y. Lanthanide double decker complexes functioning as magnets at the single-molecular level. *J. Am. Chem. Soc*. **2003**, *125*, 8694–8695, doi:10.1021/ja029629nv.
2. Rinehart, J.D.; Long, J.R. Exploiting single-ion anisotropy in the design of f-element single-molecule magnets. *Chem. Sci*. **2011**, *2*, 2078–2085, doi:10.1039/c1sc00513h.
3. Guo, F.-S.; Day, B.M.; Chen, Y.-C.; Tong, M.-L.; Mansikkamäki, A.; Layfield, R.A. Magnetic hysteresis up to 80 kelvin in a dysprosium metallocene single-molecule magnet. *Science* **2018**, *362*, 1400–1403, doi:10.1126/science.aav0652.
4. Chen, Y.-C.; Liu, J.-L.; Ungur, L.; Liu, J.; Li, Q.-W.; Wang, L.-F.; Ni, Z.-P.; Chibotaru, L.F.; Chen, X.-M.; Tong, M.-L. Symmetry-supported magnetic blocking at 20 K in pentagonal bipyramidal Dy(III) single-ion magnets. *J. Am. Chem. Soc*., **2016**, *138*, 2829–2837, doi:10.1021/jacs.5b13584.
5. Pelizzi, C.; Pelizzi, G. Investigation into aroylhydrazones as chelating agents. Synthesis and structural characterization of a tin(IV) complex with 2,6 diacetylpyridine bis(salicyloylhydrazone). *J. Chem. Soc, Dalton Trans*. **1980**, 1970-1973, doi:10.1039/DT9800001970.
6. Blessing, R.H. An empirical correction for absorption anisotropy. *Acta Crystallogr. Sect. A Found. Crystallogr.* **1995**, *A51*, 33–38, doi:10.1107/S0108767394005726.
7. Sheldrick. G. M. SHELXT—Integrated space-group and crystal-structure determination. *Acta Cryst.* **2015**, *A71*, 3–8, doi:10.1107/S2053273314026370.
8. Sheldrick. G.M. Crystal structure refinement with SHELXL. *Acta Cryst*. **2015**, *C71*, 3–8, doi:10.1107/S2053229614024218.
9. Sheldrick, G.M. A short history of SHELX. *Acta Cryst.* **2008**, *A64*, 112−122, doi:10.1107/S0108767307043930.
10. Bar, A.K.; Kalita, P.; Sutter, J.-P.; Chandrasekhar, V. Pentagonal-bipyramid Ln(III) complexes exhibiting single-ion-magnet behavior: A rational synthetic approach for a rigid equatorial plane. *Inorg. Chem*. **2018**, *57*, 2398−2401. doi.org/10.1021/acs.inorgchem.8b00059.
11. Bonardi, A.; Merlo, C.; Pelizzi, C.; Pelizzi, G.; Tarasconi, P.; Cavatorta, F. Synthesis, spectroscopic and structural characterization of mono- and binuclear iron(II) complexes with 2,6-diacetylpyridine bis(acylhydrazones). *J. Chem. Soc. Dalton Trans.* **1991**, 1063–1069, doi:10.1039/DT9910001063.
12. Bermejo, M.R.; Fondo, M.; Gonzalez, A.M.; Hoyos, O.L.; Sousa, A.; McAuliffe, C.A.; Hussain, W.; Pritchard, R.; Novotorsev, V.M. Electrochemical synthesis and structural characterization of transition metal complexes with 2,6-bis(1-salicyloylhydrazonoethyl)pyridine, H_4daps. *J. Chem. Soc. Dalton Trans*. **1999**, 2211–2218, doi:10.1039/A902018G.
13. Fondo, M.; Corredoira-Vázquez, J.; García-Deibe, A.M.; Sanmartín-Matalobos, J.; Herrera, J.M.; Colacio, E. Tb_2, Dy_2, and Zn_2Dy_4 Complexes Showing the Unusual Versatility of a Hydrazone Ligand toward Lanthanoid Ions: A Structural and Magnetic Study. *Inorg. Chem*. **2018**, *57*, 10100−10110, doi:10.1021/acs.inorgchem.8b01251.
14. Bolotina, N.B. X-ray diffraction analysis of modulated crystals: Review. *Crystallogr. Rep.* **2007**, *52*, 647–658, doi:10.1134/S1063774507040128.
15. Mondal, A.K.; Goswami, S.; Konar, S. Influence of the coordination environment on slow magnetic relaxation and photoluminescence behavior in two mononuclear dysprosium(III) based single molecule magnets. *Dalton Trans*. **2015**, *44*, 5086–5094, doi:10.1039/C4DT03620D.